Self-generated displacement current of Triboelectric Nanogenerator for Cancer Therapy: Theory and Application

Meihua Chen [1], Xin Cui [1], Yaming Zhang [1], Pingjin Zou [1], Ling Xiao [1], Mengzhe Kang [1], Junyang Chen [2], Junjin Ren [1], Zengyi Fang [1], Lijie Li [3], Jinyi Lang [1, *], Yan Zhang [1,3,4, *], and Zhong Lin Wang [4,5, *]

[1] *Department of Radiation Oncology, Radiation Oncology Key Laboratory of Sichuan Province, Sichuan Clinical Research Center for Cancer, Sichuan Cancer Hospital & Institute, Sichuan Cancer Center, School of Physics, Affiliated Cancer Hospital of University of Electronic Science and Technology of China, Chengdu 610054, China*

[2] *School of Clinical Medicine, Chengdu University of Traditional Chinese Medicine, Chendu 610072, China*

[3] *College of Engineering, Swansea University, Swansea, SA1 8EN, UK*

[4] *Beijing Institute of Nanoenergy and Nanosystems, Chinese Academy of Sciences, Beijing 100083, China*

[5] *College of Nanoscience and Technology, University of Chinese Academy of Sciences, Beijing, 100049, China*

[*]To whom correspondence should be addressed, E-mail: langjy610@163.com, zhangyan@uestc.edu.cn, and zlwang@gatech.edu

Abstract

Wearable and implantable triboelectric nanogenerators (TENGs) convert mechanical energy to electricity in daily movements of a human body. Self-generated dynamic electric field or displacement current of TENGs can operate from micrometers to centimeters, which offers a key technology for TENG-based therapy system for precision medicine on both tissues and cells. TENGs have low-current and high-voltage properties, which reduce damage to normal tissues, and kill rapidly dividing cancer cells. In this work, the dynamic electric field from TENG directly inhibit cellular proliferation behavior of cancer cells. The work paves a new way of self-generated electric field of TENG for cancer therapy.

Keywords: Triboelectric nanogenerator; self-generated electric field; cancer therapy

1. Introduction

Food and Drug Administration (FDA) approved tumor treating fields (TTFields) to use in glioblastoma multiforme (GBM), which have been found to improve survival in patients. TTFields use low-intensity (1-3 V/cm) and intermediate frequency (100-300 kHz) electrical fields to treat cancers.[1] TTFields selectively interrupt mitosis and kill rapidly dividing tumor cells by delivering continuous alternating electric fields to the tumor site.[2] As an innovative and noninvasive therapy, TTFields selectively affects dividing cells while quiescent cells are left intact. However, the treatment costs of TTFields are about $21,000 per month for prolonged treatment. The patients need to wear the TTFields device continuously with minimal interruption, for more than 18 hours a day, this inevitably requires lifestyle modifications which led to lifestyle drawbacks.[3]

Triboelectric nanogenerators (TENGs)[4] based precision medicine systems have been a wide application prospect in the medical and health field.[5] TENGs convert electricity from human biomechanical energy.[6] TENGs have been applied on peripheral nerves to modulate gastric, sciatic, and bladder function.[7] Biomechanical systems based on TENGs are effectively applied for cell modulation,[8] and direct muscle stimulation.[9] TENG based precision medicine systems have been used as prostheses for the auditory,[10] visual,[11] and olfactory systems.[12] A self-powered magnet TENG-based drug delivery system (DDS) was developed in preclinical research.[13] TENGs can controls the drug release, which is used for the DDS that transports chemotherapeutic drug doxorubicin by red blood cells (RBCs).[13]

Wearable TENGs offers novel therapeutic with self-generated fields directly treat cancer by human biomechanical energy. Yao et al. developed a human self-driven catalysis-promoting system (TENG-CatSystem) by self-generated electric field for catalytic cancer therapy.[14] TENG based devices can directly treat cancer for flexible time anti-tumor treatment. The lower frequency and higher intensity of TENG driven

by daily movement can be a great strategy for tumor treatments. In this study, we investigate that self-generated field from TENG directly treat cancer in cancer cells and murine tumors. **Figure 1** is the schematic diagram of TENG with self-generated electric field systems for cancer therapy. The TENG based electric field therapy system are shown in Figure 1a. The wearable TENG has mechanical frequency conversion and energy storage by three-dimensional (3D) printing, as shown in Figure 1b. The mechanical frequency conversion and energy storage unit of wearable TENG has the advantage of utilizing ultra-low frequency vibration to realize high-speed rotation. The unit consists of two parts: the energy storage and the mechanical frequency conversion part. The energy storage part is an eccentric rotor structure and vibrates in response to ultra-low frequency excitation. The mechanical frequency conversion part converts the vibration into high-speed rotation.[15] This work can pave a new way for the flexible, stretchable, and fully biodegradable TENG with self-generated electric field systems for cancer treatment.

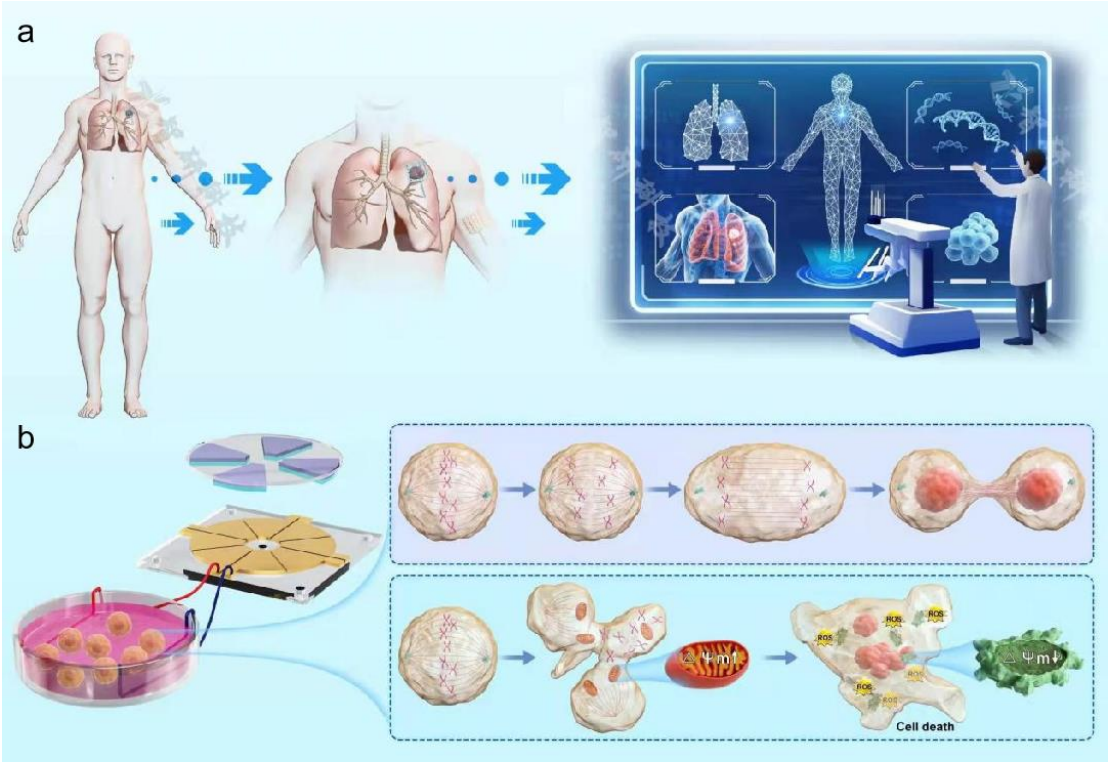

Figure 1. Schematic diagram of TENG with self-generated electric field systems for cancer therapy. a. TENG based electric field therapy system. b. Cell division and mitochondria function of cancer cells under TENG-driven electric stimulation.

2. Theory of triboelectric nanogenerators

While triboelectric charges occur on surfaces simply due to contact electrification for two different materials, an additional term $\boldsymbol{P}_s$, mechano-driven produced polarization, is added by Wang [16]

$$\boldsymbol{D} = \varepsilon_0 \boldsymbol{E} + \boldsymbol{P} + \boldsymbol{P}_S, \tag{1}$$

where, $\boldsymbol{P}$ is the first term polarization vector induced by an external electric field, depend on the surface charges and the relative movement of the media. According to Equation (1) and Maxwell's equations, define

$$\boldsymbol{D}' = \varepsilon_0 \boldsymbol{E} + \boldsymbol{P}, \tag{2}$$

For slow-moving media system with acceleration and time-dependent configuration, the Maxwell's equation is given by:[17]

$$\nabla \cdot \boldsymbol{D}' = \boldsymbol{\rho}_f - \nabla \cdot \boldsymbol{P}_S \tag{3a}$$

$$\nabla \cdot \boldsymbol{B} = \boldsymbol{0} \tag{3b}$$

$$\nabla \times (\boldsymbol{E} + \boldsymbol{v}_r \times \boldsymbol{B}) = -\frac{\partial}{\partial t}\boldsymbol{B} \tag{3c}$$

$$\nabla \times [\boldsymbol{H} - \boldsymbol{v}_r \times (\boldsymbol{D}' + \boldsymbol{P}_S)] = \boldsymbol{J}_f + \boldsymbol{\rho}_f \boldsymbol{v} + \frac{\partial}{\partial t}[\boldsymbol{D}' + \boldsymbol{P}_S] \tag{3d}$$

where $\boldsymbol{v}$ and $\boldsymbol{v}_r$ is the translation moving and rotation velocity of the medium, respectively. These equations are fundamentals for describing the coupling among mechano-electric-magnetic multi-fields for TENG, including electromagnetic interaction and power generation .

3. Results and discussion

3.1. Solutions of self-generated field of TENG

3.1.1 The electric field of two charged parallel wire

The two infinite long wires of same radius R, with the same line charge density, and opposite polarity is parallel and has a distance D. While the charge density of two long wire is λ and $-\lambda$, and $R \ll D$ for cancer therapy, using the mathematical derivation in Appendix A, the total electric field at a distance r from the wire A is:

$$E = \frac{\lambda D}{2\pi\varepsilon_0 r(D-r)}\hat{r}_{AB} \quad 0 < r < D \tag{3}$$

where $\hat{r}_{AB}$ is unit vector point from A to B. The electric field produced by two parallel wires is point from A to B, the min electric field appear at $r = \frac{D}{2}$, the electric field value is $E_{\min} = \frac{2\lambda}{\pi\varepsilon_0 D}$.

3.1.2 The electric field of two charged curved surface

The capacitor model composed of two charged curved surfaces. The radius of electrodes is unity. The upper and lower electrodes are defined by $\phi_0 \le \phi \le \phi_1$, and $-\phi_1 \le \phi \le -\phi_0$, respectively. The potential φ produced by the charged curves surface of TENGs satisfies 2D Laplace equation.[18] The general solution of Laplace equation is

$$\varphi_i = \sum_{n=1}^{\infty} a_n \rho^{(-1)^i n} \sin(n\phi), \quad i = 1, 2, \tag{4}$$

where a_n are constants. The i (1 and 2) stands for the region of $\rho > 1$ and $\rho \le 1$. By using the mathematical derivation shown in Appendix A, we have:

$$E = -\nabla\varphi(\rho,\phi) = -\left(\frac{\partial\varphi}{\partial\rho}\hat{e}_\rho + \frac{1}{\rho}\frac{\partial\varphi}{\partial\phi}\hat{e}_\phi\right) = -\sum_{n=1}^{\infty} n a_n \rho^{n-1}[\sin(n\phi)\hat{e}_\rho + \cos(n\phi)\hat{e}_\phi] \tag{4}$$

where $\hat{e}_\rho$ and $\hat{e}_\phi$ is the unit vector of electric field in polar coordinates. The electric field distribution is depended on the angle ϕ_0 and ϕ_1.

3.2.Fabrication and performance of TENG

The schematic of the structure of TENG is shown in **Figure 2a**. Wearable TENG is

currently recognized as one of the most practical solutions to achieve seamless combination of TENG and human movement.[19] TENGs possess the ability to transform diverse body movements into electrical signals, opening up possibilities for innovative self-powered biomedical applications.[20] The working principle of this TENG is shown in Figure 2b. Based on triboelectrification and electrostatic induction, electrons flow back and forth between the two groups of electrodes through an external circuit. The potential distribution is simulated by COMSOL, as shown in Figure 2c. The output characteristics of the TENG are shown in Figure 2d-f. The open-circuit voltage (V_{oc}) can reach up to 650 V at a rotation speed of 600 rpm, as shown in Figure 2d. The short-circuit current (I_{sc}) is 4 μA at a rotation speed of 600 rpm, as shown in Figure 2e. The output is constant within 2 h, as shown in Figure 2f. The output charge is ~45 nC at a rotation speed of 200 rpm (Figure S1a, Supplementary Information). The output charge remains stable with rotational speed from 200 to 600 rpm. Open circuit voltage at 200 rpm is 520 V (Figure S1b, Supplementary Information).

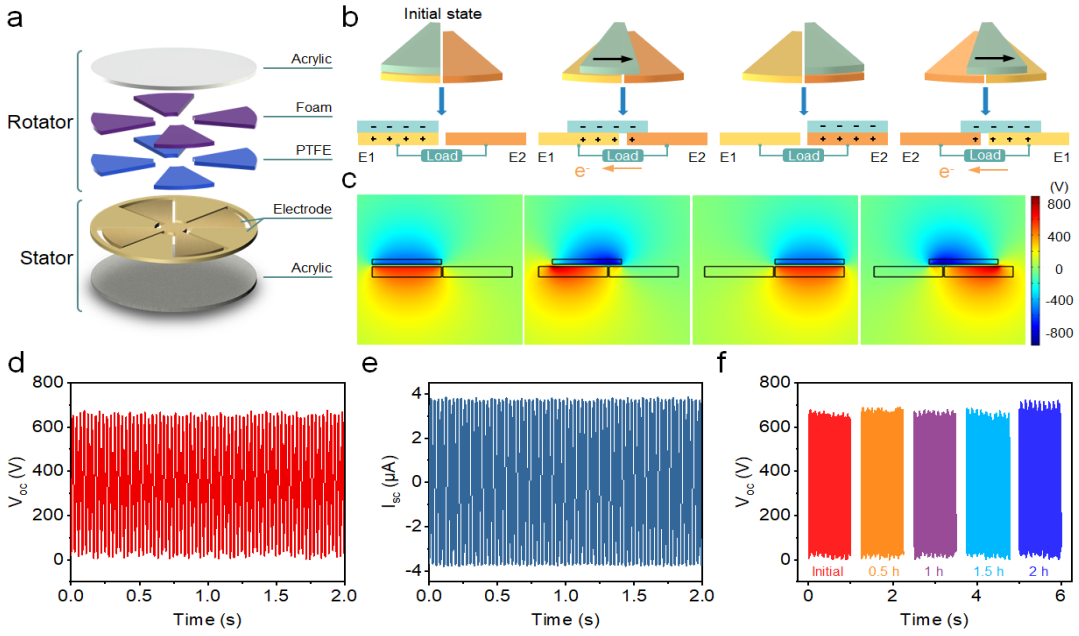

Figure 2. Electrical output performance of TENG. a. Schematic structure of the TENG. b. The working principle of TENG. c. The potential distribution is simulated by COMSOL. d. Open-circuit voltage, and e. short-circuit current of TENG with various rotation rates. f. The stability of open-circuit voltage over 2 hours.

Since the internal resistance of the TENG is relatively large, usually between tens of MΩ and hundreds of MΩ.[21] The impedance of tumor tissue in mice is about a few tens of kΩ.[22] The distance between the insulated wires is 1 cm. After connecting the device, a field of only 0.26 V/cm is generated in the area of interest. Self-generated electric field of TENGs at low intensity of 0.26 V cm^{-1} can kill rapidly dividing cancer cells. Thus, the currents are suitable for cellular electrical stimulation to inhibit cancer cell growth in vitro. TENGs offer distinct advantages over traditional electric stimulators for in vivo biomedical applications, characterized by high voltages and low current outputs that ensure excellent biosafety and suitability for in vivo utilization. TENGs have low-current properties also can reduce damage of normal tissue in vivo. The lower current TENG for cancer therapy are novelty compared high output of previous works.

Previous approaches of self-powered TENG-based electric stimulation system can enhance the proliferation of fibroblast cells with the ranges of currents between 10 and 50 μA.[8b] TENG can effectively convert mechanical energy to electric with high power density. Because the energy, frequency, and acceleration of human movement are limited, the development of the self-generated electric field of TENG with low-current is key for therapy and health monitor. TENGs operating at low frequencies (a few Hz) enable direct application without the need for external energy transmitters, simplifying therapy procedures.[14] Saqib et al. developed a highly efficient TENG that captured energy from omnidirectional movements within the human body using cellulose-based particles in rapidly degradable gelatin capsules as friction anode and cathode layers, achieving a power range of 5.488 to 70 μW and a maximum energy conversion efficiency of 74.35%.[23] Park et al. ingeniously harnessed friction-generated electric charge in the human body to create simplistic aluminum electrode TENGs, where each step generated ample power to instantaneously illuminate 100 commercial LEDs.[24] The energy generated by low-frequency energy TENGs during daily movements is sufficient for direct cancer cell killing. Recent studies have shown that cancerous cells

are more susceptible to death comparing normal cells under specific ES conditions.[25] Mild ES (at ≈1.2 V) induced pronounced double strand breaks and adenine base damage in cancer cell DNAsfor killing cancer cells.[26] TENG-based electrotherapeutic platforms that produced current stimulation at 150 μA, effectively disrupt actin and tubulin-related cellular cytoskeleton, reducing in vitro cell migration without apparent toxicity to normal organs and tissues. Furthermore, TENG-based treatments with the current stimulation at 150 μA prevented early spreading of cancer cells to other body sites.[27] Typical output characteristic of TENG is low current in wearable applications.

In specific experimental setups, it is crucial to implement suitable circuitry or energy management systems to facilitate the direct application of the self-generated dynamic electric field of TENGs. This includes the conversion from AC to DC, which is particularly relevant for electrotherapy approaches relying on continuous DC current. By integrating rectification and energy storage components, practical solutions can be achieved, overcoming limitations related to size and energy conversion efficiency.[28] Recent studies have introduced semiconductor-based DC-TENGs, which operate on the tribovoltaic effect, akin to the photovoltaic effect but utilizing friction as the energy source.[29] These DC-TENGs leverage semiconductor materials with low impedance (~ kΩ), enabling them to generate high current (~A m^{-2}).[30] They use the inherent triboelectric charges as mobile charges, which canbe directly driven by the built-in electric field in p-n junction or Schottky junction to produce a DC output.[30-31]

3.3.TENG-driven well plates for cell test

We designed a self-generated electric field system with the assistance of TENG for cancer therapy (**Figure 3a**). Cells are seeded at the bottom of the pink chamber (Figure 3b), and the device was connected to the TENG via a pair of copper electrodes (Figure 3c). To optimize the electrodes, the potential distribution and electric field distribution of a 24-well plate were simulated using COMSOL. In the simulations, the electrode with an arc of 82 degrees exhibited the best electric field distribution than the electrodes with other arcs (Figure 3d). Subsequently, we simulated the potential distribution and

electric field distribution of 24-well plates under an applied voltage of 600 V (Figure 3e). The electrode structure design can effectively optimize the electric field distribution to improve the outcome of self-generated electric field.

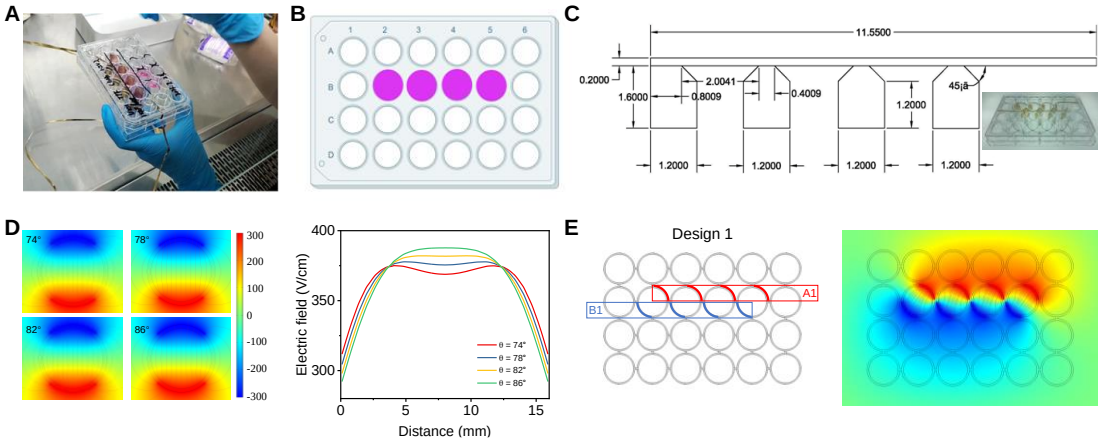

Figure 3. Optimization of electric field distribution. a. Optical photograph of a copper electrode array in a 24-well plate. b. Schematic illustration of the 24-well plate. Cells are seeded on the bottom of the pink chamber. c. Structural design of the copper electrode array. d. Electric field distribution under different electrode arcs. e. Electric field distribution and potential distribution of the electrode array at 600V.

3.4.*In vitro* cancer therapy

Figure 4a is the schematic diagram of TENG with self-generated electric field systems on cancer cells in vitro. The electric stimulation driven by TENG effectively controls the cell growth and proliferation of melanoma cell line (B16F10), as shown in Figure 4b. The cancer cells were stimulated directly by the TENGs for 2 h and further incubated for another 24 h. Then CCK-8 assay was carried out to evaluate the effect of the electric fields on tumor cell proliferation. Compared to the untreated cells, the viability of B16F10 cells treated with TENG stimulation decreased by 82%. To rigorously assess the tumor-killing effects of TENGs, a control group employing a conventional signal generator was included. The cancer cell killing efficiency of the conventional signal generator (0.26 V/cm at 100 kHz for 2 hours) group was 6%, indicating the limited effect of conventional pulse electric fields alone (Figure S2, Supplementary Information). We investigate the inhibitory effects on cancer cells of

different treatment times in B16F10 cells in 2D culture model. The anti-tumor effects were increased with the prolongation of treatment and reached the plateau at 2 hours, as shown in Figure 4c. The inhibitory effect of different electric field intensities on tumor cell growth is also studied as shown in Figure 4d. As treatment efficacy was positively correlated with TTFields intensities,[2a, 2b] the B16F10 cells were exposed to various intensities between 0.1 V cm^{-1} and 1.8 V cm^{-1}. We found that TENG with self-generated electric field at low intensity of 0.26 V cm^{-1} has significant enhanced anti-tumor effect compared to the lower intensity of 0.15 V cm^{-1} ($p < 0.001$). When the electric field intensity is greater than 0.26 V cm^{-1}, the inhibitory effect was saturated at lower electric field. The efficacy, reliability, and safety of TTFields therapy are contingent upon specific parameters.[2a, 2b] Researchers have explored multiple parameters to optimize the therapeutic potential of TTFields for cancer cell eradication.[32] TTField inhibition exhibits distinct dependencies on intensity and frequency across different cancer cell types. For the treatment of malignant melanoma, optimal parameters for electric field therapy include a frequency of 100 kHz and intensity ranging from 1 to 2 V/cm.[2a] Moreover, the effectiveness of TTFields is influenced by the relative alignment of the mitotic axis and the field vector.[32] TTFields therapy utilizes low-intensity, alternating electric fields as the predominant waveform. With microsecond-range pulse width, these fields effectively disrupt cell division by significantly impacting the interaction with tumor cells.[2a, 2b] This work demonstrates that TENGs can generate self-generated electric fields at a low intensity of 0.26 V/cm, offering the potential for selective eradication of rapidly dividing cancer cells. Thus, the currents driven by TENG hold promise for in vitro cellular electrical stimulation, effectively inhibiting cancer cell growth. Additionally, TENGs exhibit low-current properties, minimizing the risk of normal tissue damage in in vivo applications. This novel approach employing lower current TENGs for cancer therapy represents a significant advancement in contrast to previously reported high-output methodologies.

The effects of TTFields, primarily affecting mitotic cells, were proposed to involve the alignment of proteins with large dipole moments, for example, tubulin dimers,

compromising the mitotic spindle and the mitotic process.[2] Strong forces on septin molecules were suggested to induce apoptotic cell death. Additionally, the electric fields were proposed to become highly inhomogeneous at the mitotic furrow during telophase, influencing biomolecules in that region and compromising cell division. Understanding these mechanisms is crucial for optimizing electric field-based therapies and improving treatment outcomes. The effect of self-generated electric fields on cancer cells was assessed through various analyses. The apoptosis of different cancer cells was assessed by annexin V/PI double staining and quantified by subsequent flow cytometric analysis. For B16F10 cells, a striking increase in apoptosis was observed after treatment, the apoptosis rate reached 66.8%. Representative flow cytometry images are shown in Figure 4e, apoptotic cells populate the upper (late apoptosis) and lower (early apoptosis) right quadrants. These tumor cells presented marked reductions in proliferation and increased apoptosis after the TENG with electric fields treatment. In order to analysis cellular oxidative damage, we measured cellular levels of 8-hydroxy-2'-deoxyguanosine (8-OHdG, indicator of oxidative DNA damage), 4-hydroxy-2-nonenol (4HNE, an indicator of lipidperoxidation), protein carbonyl (PCO, a biomarker of protein oxidation), before and after self-generated electric field of TENG treatment. Figure 4f shows 8-OHdG, 4HNE and PCO amounts were significantly increased in treated B16F10 cell lysates compared to controls. Live/dead cell fluorescence staining was shown in Figure 4g. By comparing the number of dead cells with the total amount of cells, the dead cell percentage was calculated. For B16F10 cells, the dead cell percentage is at 75.1%.

Programmed cell death is indicated by a depolarization of mitochondrial membrane potential (MMP) which has been examined by JC-1 staining.[34] As shown in Figure 4h, severe mitochondria depolarization was observed in cancer cells under electric field of TENG, with an increase in green/red fluorescence ratio. The green: red ratio of B16F10 cells reached 6.6. Mitochondrial dysfunction results in ROS accumulation.[34] By analyzing the levels of intracellular ROS by H2CDFDA staining, we found that self-generated electric field of TENG induced the accumulation of ROS

in cancer cells, as shown in Figure 4j. Intracellular ROS levels are affected by cell membrane damage and intracellular Ca^{2+} concentrations. The evolution of intracellular Ca^{2+} levels was studied in cancer cells using Fluo4-AM as a fluorescent calcium probe. Intracellular Ca^{2+} level was 2.2-fold higher than the cases without treatment for B16F10 cells, as shown in Figure 4i. These findings demonstrate that the self-generated displacement current of TENG effectively impeded the proliferation of cancer cells. The TENG-driven stimulation resulted in cell apoptosis, accompanied by increased ROS accumulation and calcium overload. These compelling findings elucidate the profound impact of TENG-driven high voltage low current stimulation on cancer cell viability, achieved through mitochondrial dysfunction and heightened oxidative damage at the cellular level.

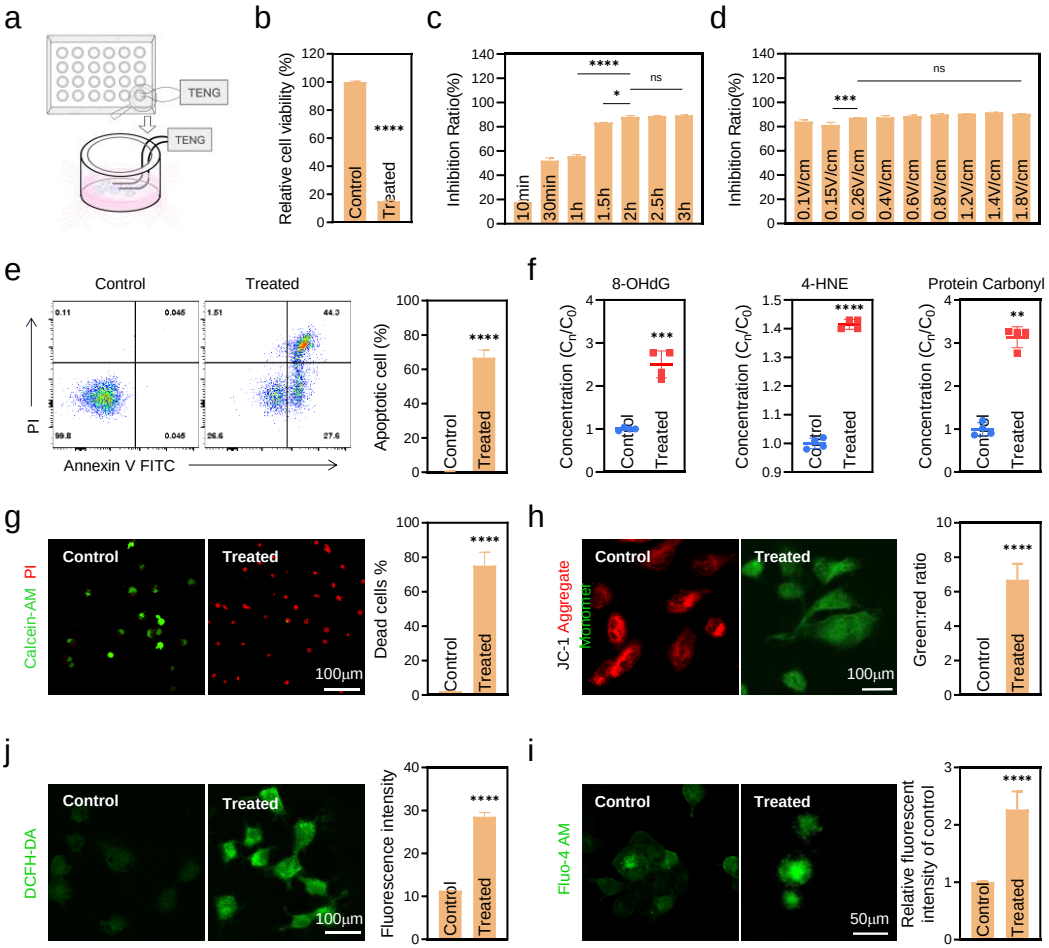

Figure 4. TENG based self-generated electric fields inhibit tumor growth in vitro. a.

Schematic of the in vitro experimental setup for TENG based self-generated electric field systems. b. Relative cell viabilities of B16F10 cells 24h after treatment with TENG based self-generated electric field systems (n = 4). c. The inhibition ratio of different treatment time of TENG with self-generated electric field in B16F10 cells (n = 4). d. The inhibition ratio of different electric field intensities of in B16F10 cells (n = 4). e. Representative flow cytometry profiles and apoptotic cell percentage for B16F10 cells under TENG based self-generated electric fields (n = 4). f. Levels of 8-hydroxy-20-deoxyguanosine (8-OHdG), 4-hydroxynonenal (4-HNE), and protein carbonyl (PCO) content after different treatments (n = 4). g. Calcein AM and PI double-stained images of B16F10 cells treated with TENG based self-generated electric fields (n = 4). h. Fluorescence images and the ratio of fluorescence intensity of JC-1 monomers and JC-1 aggregates of the B16F10 cells under different treatments (n = 4). i. Representative fluorescent images and quantification of H2DCFDA staining for intracellular ROS (n = 4). j. Representative fluorescent images and quantification of staining for intracellular Ca^{2+} and the intensity of fluorescence (n = 4). Statistical significance was calculated via Student's t-test compared with the control or the ordinary one-way ANOVA with multiple comparisons. Values of $p < 0.05$ were considered statistically significant. Asterisk (*) denotes statistical significance between bars (*$p < 0.05$, **$p < 0.01$, ***$p < 0.001$, ****$p < 0.0001$); ns, not statistically significant.

3.5. *In vivo* cancer therapy

We next evaluated the in-vivo antitumor efficacy of the TENG with self-generated electric field by using murine tumor models. C57BL/6 mice were inoculated subcutaneously with B16F10 malignant melanoma cells. One day after tumor inoculation, a pair of 10-mm long, entirely insulated wires with a diameter of 0.25 mm were on both sides of the tumor, as shown in **Figure 5a**. Treatment began one day after tumor cell inoculation and performed daily for six days. According to the experiments of TTFields originally proposed by Kirson et al., the use of parallel wires in in vivo cancer therapy serves the purpose of generating alternating electric fields.[2a] TTFields,

delivered through insulated electrodes with parallel wire configuration, exert inhibitory effects on dividing cancer cells by generating alternating electric fields. This parallel wire setup enables the creation of a homogeneous electric field near the tumor. Targeted delivery of electric fields directly to the tumor region is ensured. Notably, in addition to electric field generation, the parallel wire configuration enables the generation of low current as electrons flow along the wires[35]. This current can be harnessed for the purpose of targeted cell killing, with the parallel wires acting as electrodes to deliver low current to the tumor site. By incorporating parallel wire setups in in vivo cancer therapy, a dual-mode functionality is achieved. The parallel wires can generate low current for targeted cell killing, while the electric field selectively affects dividing cells within the tumor. This combination of current and electric field offers a comprehensive approach to enhance treatment efficacy and selectivity. Representative photographs of the posttreatment observation phase are shown in Figure 5b. We found that TENG with self-generated electric field at low intensities of 0.26 V cm^{-1} effectively inhibited malignant melanoma growth by comparing nontreated control. Treated tumors were significantly smaller comparing with control tumors at the end of observation period. Figure 5c shows the tumor volume curves of treated side and control side. Figure 5d represent the mean tumor volume of each side at the end of observation (n = 5 mice, p = 0.0005; paired t-test). Tumor growth inhibition rate (TGI, %) was 44.99% for tumors by self-generated electric field of TENGs. There are control groups for in vivo experiments that are completely untreated by electric fields (Figure S3, Supplementary Information). From representative photographs of the posttreatment observation phase (Figure S3b, Supplementary Information), the control group tumors are not affected by the electric field. The tumor growth curves show untreated control and treated group (Figure S3c, Supplementary Information). In the animal experiments, the body weights of mice kept constant (Figure S4, Supplementary Information). Following the 7-day observation period, tumor tissue and adjacent tissues were collected for histologic analyses. In optical images, tissues of treated sides stained with hematoxylin-eosin and Ki-67 immunohistochemistry confirmed the inhibition of the growth of malignant cells

(Figure 5e and 5f). No notable adverse effects were observed on gross health measures, blood routine (Figure S5, Supplementary Information), blood biochemistry (Figure S6, Supplementary Information), and histological analysis of the major organs (Figure S7, Supplementary Information).

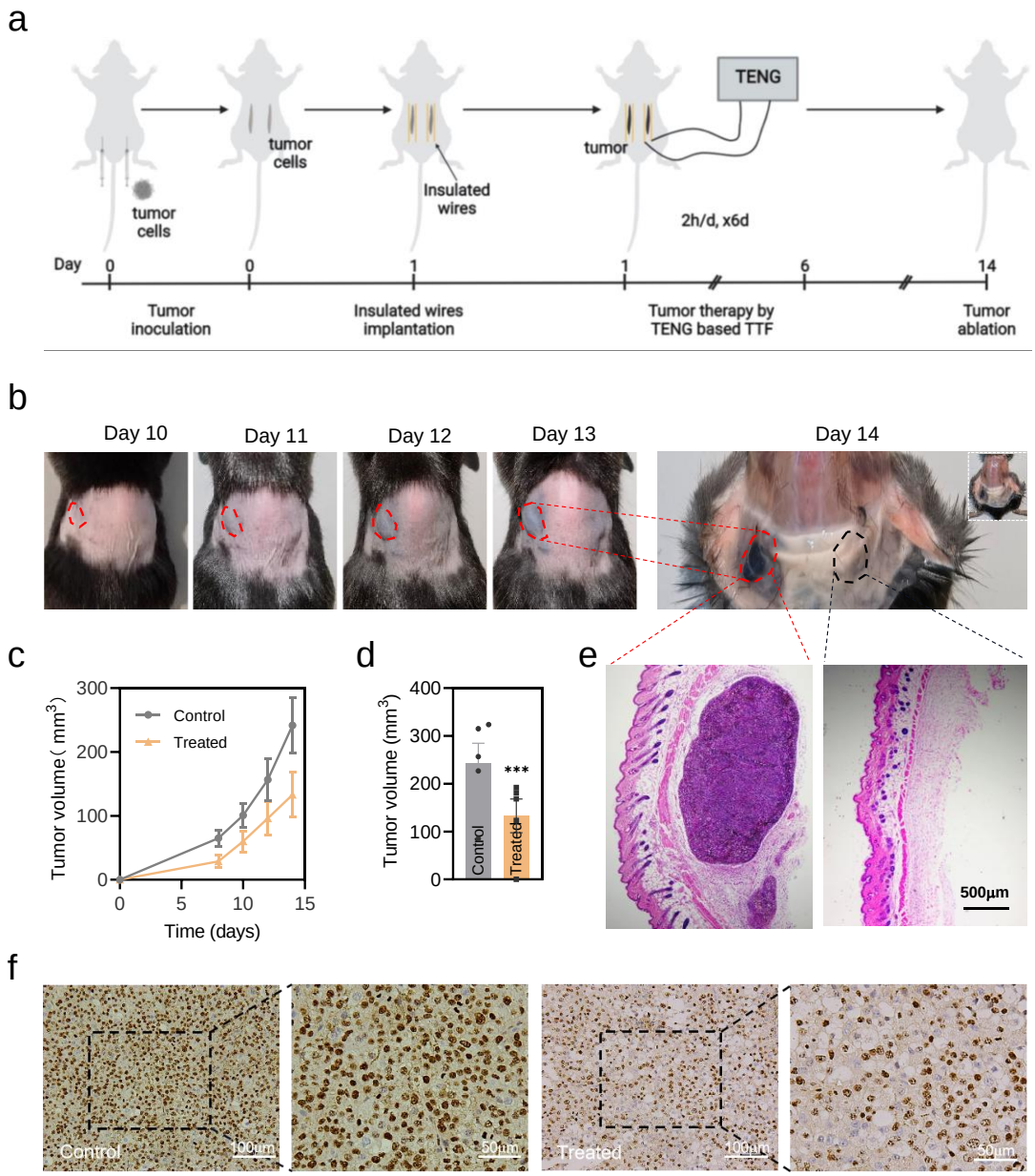

Figure 5. Anti-tumor effect of self-generated electric field of TENG in vivo. a. Schematic illustration of the in vivo experiments of TENG with self-generated electric field. b. Photographs for treated tumors and control tumors of B16F10 tumor-bearing mice at observation period. c. Tumor volume curve of each group after tumor inoculation (n = 5). d. Tumor volume of each group of B16F10-bearing mice on the

14th day after tumor inoculation (n = 5). e. HE staining for tissues of untreated side and treated side in B16F10 tumor-bearing mice. Scale bars, 500μm. f. Ki-67 staining for tissues of untreated side and treated side in B16F10 tumor-bearing mice. Scale bars, 100μm, bars in high-magnification panels, 50μm. Statistical significance was calculated via Student's t-test, and $p < 0.05$ was considered statistically significant. Asterisk (*) denotes statistical significance between bars (***$p < 0.001$) conducted using Graphpad Prism 8.

Electrical stimulation (ES) has been applied to regulate cellular activities in tissue engineering.[36] Electric fields have been applied in clinical cancer therapy through mechanisms of irreversible electroporation, electric field-induced mitosis inhibition, and electrochemotherapy.[37] By changing parameters, electric fields can directly kill of cancer cells.[37] However, it faces great challenges of limited efficacy in certain tumor types, limited penetration depth, compliance and treatment burden, and adverse effects and device-related issues.[38] To improve usability, TTFields devices are designed to be wearable and portable, causing minimal disruption to daily activities. TENGs offer unique advantages for cancer treatment, including wearability, self-powering, flexibility, and high biosafety.[4a, 9b, 37] Unlike other ES techniques, TENGs convert mechanical energy from daily human movements into electrical impulses, eliminating the need for external power sources. TENGs can be integrated into wearable devices, allowing for portable and continuous therapy while maintaining patients' daily activities. Previous studies have demonstrated the potential of TENGs in personalized long-term treatment, such as neural interfacing,[39] tactile restoration,[40] and bone repair.[41] The self-generated electric fields of TENGs selectively target cancer cells, minimizing damage to healthy cells and reducing side effects associated with non-targeted ES. Implantable TENGs, when excited by ultrasound, can generate AC voltage and release anti-mitotic drugs into tumor tissues, enhancing cell death synergistically.[42] TENG-based therapy systems can be easily integrated with other therapeutic modalities, such as DDS or imaging technologies, enabling combination therapies for enhanced treatment efficacy.[43]

Challenges in TENG-based therapy systems include low energy density. Recent studies have made progress in addressing these challenges, such as fabricating smaller TENGs using 3D printing, improving energy collection efficiency through flexible materials, and enhancing device durability through encapsulation and protective coatings.[44] Long-term and reliable operation of TENG devices is crucial for biomedical applications, and research has focused on developing long-term implantation options.[39-41] Accurate DDSs are crucial for minimizing side effects and improving treatment efficacy. TENG-based devices have been developed to harvest energy and enable electrical stimulation of cancer cells, leading to significant drug absorption.[45] Scalability and cost-effectiveness of the manufacturing process are important considerations for market applications. Scalable fabrication techniques have been explored to enable large-scale manufacturing of TENG devices.[46]

In this study, we demonstrate the novel approach of utilizing TENGs to generate self-generated electric fields and low current for cancer treatment. TENGs offer advantages such as self-powered operation, portability, and potential for wearable applications. The self-generated electric field of TENG is safe for cancer therapy. By selectively affecting dividing cells while leaving quiescent cells intact, TENG with self-generated electric field can directly induce cell cycle arrest and apoptosis in cancerous cells. Wearable TENG devices can prevent fibrosis induced by foreign body reactions in the surrounding tissue. Additionally, the self-generated electric field of TENG allows for easier displacement from treatment sites, which is beneficial for small-sized devices. TENG also enables close monitoring of cytotoxicity and histocompatibility. Thus, direct utilization of TENGs' self-generated electric field enhances therapy systems' efficiency, cost-effectiveness, portability, and safety. TENG-based therapy systems provide direct and localized therapeutic effects, eliminating the need for additional power sources. Their lightweight nature and seamless integration into wearables enable portable and continuous treatment. Moreover, TENG-based systems offer non-invasive and targeted treatment options, reducing potential side effects. Except the effect of self-generated dynamic electric field on cancer cells, its low-current properties and the

principles underlying these effects may have implications for reducing damage to normal tissues and promoting cell regeneration in other contexts, including acute renal injury.[47] Recent advances in TENG have significantly promoted wound healing by simulating the natural healing mechanism of endogenous electric fields.[48] These TENGs also have potential applications in wound treatment, nerve stimulation, and tissue regeneration. These advancements in TENG-based systems hold promise for improving therapeutic outcomes and expanding practical applications.

4. Conclusion

In summary, we demonstrate that TENG with self-generated electric field can effectively inhibit tumor cells growth in vitro and in vivo. The TENG can offer a high and consistent electricity output to hinder the proliferation of cancerous cells. The stimulation induced cell apoptosis as ROS accumulation and calcium overload. These findings demonstrate how TENG-driven high voltage low current stimulation significantly decrease cancer cell viability by mitochondrial dysfunction and enhancing oxidative cellular damage. Murine melanoma cancer was efficiently suppressed by self-generated electric field of TENG in vivo. This work can enable self-powered stimulator for wearable and chronically implantable electrical cancer treatment system.

5. Experimental Sections

Fabrication of TENG: The TENG was based the 80 μm-thick PTFE film and the stator with copper electrodes. A disk-shape acrylic board was used as the substrate with a diameter of 80 mm. The foam was cut into radial-arrayed sectors of 45 degree. The outer and inner diameters of the sectored foam are 80 mm and 32 mm, respectively. Four sectored foams were adhered to the acrylic substrate to achieve soft contact, and the PTFE film was adhered to the foams as a triboelectric layer. For the stator, complementary sector-shaped copper electrodes were glued to an acrylic plate with the size of 100 mm × 100 mm × 4.5 mm. The rotary motion was driven by a stepping motor.

Measurement of the output of the TENG: A programmable electrometer (6514, Keithley Instruments model) was used to test the V_{OC} and I_{SC} of TENG.

Cell cytotoxicity tests: Cell cytotoxicity tests was conducted using a cell counting kit-8 (CCK-8; Solarbio, China) and Calcein-AM/Propidium Iodide (Calcein-AM/PI; Solarbio, China) Double Stain Kit.

Detection of intracellular ROS levels: The ROS-sensitive probe H2DCFDA (HY-D0940, MCE, China) was employed. In brief, tumor cells were seeded into a 24-well plate (1×10^4 cells per well) and stimulated with TENG for 2h. Afterward, the cells were incubated with 10 μM H2DCFDA at 37 ℃ for 30 min, and confocal laser fluorescence imaging (CLSM) was performed. Image processing and data analysis were performed using ImageJ.

Measurement of mitochondrial membrane potential: Cells were seeded into a 24-well plate and subjected to TENG-driven stimulation for 2 h. Thereafter, cells were stained with JC-1 according to the manufacturer's protocols. The samples were then imaged by LSM170 confocal microscopy (Zeiss).

Intracellular Ca^{2+} concentration analysis: The intracellular Ca^{2+} concentration was detected using the indicator dye fluo-4 AM (Solarbio, Beijing, China). Cancer cells were incubated with 4 μM Fluo-4-AM in HEPES buffered saline for 60 min at 37 ℃ in 5% CO_2, and CLSM was performed.

Animals: Six-to-eight week old female BALB/c mice were purchased from Beijing HFK Bioscience Co., Ltd. (www.hfkbio.com), and the procedures for handling the animals were performed firmly according to the national standards "Laboratory Animal Requirements of Environment and Housing Facilities (GB 14925-2001)". Animal experiments were approved by the ethics Committee for Medical Research and New Medical Technology of Sichuan Cancer Hospital (Approval Number: SCCHEC-04-2022-011).

In vivo cancer therapy: The mice were shaved, depilated, and disinfected on the back under isoflurane anesthesia. The spinal column was used as the central axis, tumor cell line inoculums were injected (25 μl; 3×10^5 cells) subcutaneously into both sides at an

interval of ~15 mm. One day later, 10-mm-long pairs of parallel, insulated wires (outer diameter, 0.25 mm; insulation thickness, 0.125 mm; Tefzel) placed intradermally into both sides of the tumor. Mice were treated daily for 6 consecutive days. Each treatment session lasted for 2 h. After treatment, the implanted wires were removed. Tumor growth was monitored for 7 consecutive days and photos were taken as indicated. Tumors were measured using a caliper. The tumor volume was calculated as follows: tumor volume (mm^3) = 1 × (2 ×length × width × height)$^{-1}$. Tumor growth inhibition rate is calculated as (mean tumor $volume_{control}$−mean tumor $volueme_{treated}$)/mean tumor $volume_{control}$ × 100%. When the observation was finished, the mice were euthanized, the skin overlaying the tumor was removed, tumors were harvested, fixed in paraformaldehyde, and paraffin embedded. To evaluate the possible adverse effects of electric field therapy on mice, each mouse was weighed every two days. Furthermore, the mice's fur ruffling, behavior, and feeding were continuously observed. Tumor-burdened and non-tumor-bearing control mice were treated with electric field therapy and analyzed at the end of observation on hematology, blood biochemistry and pathology of the major organs.

Statistical analysis: All data are expressed as mean ± s.e.m., n = 4 and 5 for correspond to in vitro and in vivo experiments, respectively. All statistical tests were performed with GraphPad Prism 8.0 software. Statistical significance was calculated via Student's t-test compared with the control or the ordinary one-way ANOVA with multiple comparisons. Values of $p < 0.05$ were considered statistically significant. Asterisk (*) denotes statistical significance between bars (*$p < 0.05$, **$p < 0.01$, ***$p < 0.001$, ****$p < 0.0001$); ns, not statistically significant.

Supporting Information

Supporting Information is available from the Wiley Online Library or from the author.

Acknowledgement

The authors are thankful for support from Major Program of National Natural Science

Foundation of China (Grant No. 52192610, 52192612) and Key Program of National Natural Science Foundation of China (Grant No. U22A2077). The authors are thankful for the support by the Fundamental Research Funds for the Central Universities (Grant No. ZYGX2021YGCX001, ZYGX2015KYQD063). The authors are thankful for the support from the Science and Technology Department of Sichuan Province (Grant No. 2023NSFSC0708).

Declaration of Competing Interest

The authors declare that they have no known competing financial interests or personal relationships that could have appeared to influence the work reported in this paper.

Credit authorship contribution statement

Meihua Chen: Conceptualization, Methodology, Formal analysis, Data curation, Writing original draft, Validation; **Xin Cui:** Conceptualization, Methodology, Formal analysis, Data curation, Writing original draft, Validation; **Yaming Zhang**: Methodology, Formal analysis, Data curation, Writing original draft; **Pingjin Zou:** Methodology, Formal analysis, Validation; **Ling Xiao:** Methodology, Formal analysis, Validation; **Mengzhe Kang:** Methodology, Formal analysis, Validation; **Junyang Chen:** Methodology, Formal analysis, Validation; **Junjin Ren:** Methodology, Formal analysis, Validation; **Zengyi Fang:** Methodology, Formal analysis, Validation; **Lijie Li:** Methodology, Formal analysis, Writing-reviewing and Editing; **Jinyi Lang:** Conceptualization, Methodology, Supervision, Formal analysis, Writing-review & editing; **Yan Zhang:** Conceptualization, Methodology, Supervision, Formal analysis, Writing-review & editing; **Zhong Lin Wang:** Conceptualization, Methodology, Supervision, Formal analysis, Writing-review & editing.

Data Availability Statement

The data that support the findings of this study are available from the corresponding

author upon reasonable request.

Appendix A

The two infinite long wires of same radius R, with the same line charge density, and opposite polarity is parallel and has a distance D. While the charge density of two long wire is λ and $-\lambda$, and $R \ll D$ for cancer therapy, the electric field vectors at a distance r from the wire A, produced by the two parallel wires are:[49]

$$E_A = \frac{\lambda}{2\pi\varepsilon_0 r}\hat{r}_{AB} \tag{A1a}$$

$$E_B = \frac{\lambda}{2\pi\varepsilon_0 (D-r)}\hat{r}_{AB} \tag{A1b}$$

Where $\hat{r}_{AB}$ is unit vector point from A to B. The total electric field at a distance r from the wire A is:

$$E = E_A + E_B = \frac{\lambda D}{2\pi\varepsilon_0 r(D-r)}\hat{r}_{AB} \quad 0 < r < D \tag{A2}$$

The electric field produced by two parallel wires is point from A to B, the min electric field appear at $r = \frac{D}{2}$, the electric field value is $E_{\min} = \frac{2\lambda}{\pi\varepsilon_0 D}$.

The capacitor model composed of two charged curved surfaces. The radius of electrodes is unity. The upper and lower electrodes are defined by $\phi_0 \le \phi \le \phi_1$, and $-\phi_1 \le \phi \le -\phi_0$, respectively. The potential φ produced by the charged curves surface of TENGs satisfies 2D Laplace equation.[18] The general solution of Laplace equation is

$$\varphi_i = \sum_{n=1}^{\infty} a_n \rho^{(-1)^i n} \sin(n\phi), \quad i = 1, 2, \tag{A3}$$

The i (1 and 2) stands for the region of $\rho > 1$ and $\rho \le 1$. The boundary conditions of potentials at $\rho = 1$ for the upper electrodes ($\phi \ge 0$) are:

$$\varphi_1(1, \phi) = \varphi_2(1, \phi) \quad \phi \in (\phi_0, \phi_1), \tag{A4}$$

$$\left.\frac{\partial\varphi_1(\rho,\phi)}{\partial\rho}\right|_{\rho=1}=\left.\frac{\partial\varphi_2(\rho,\phi)}{\partial\rho}\right|_{\rho=1},\quad \phi\in[(0,\phi_0)\bigcup(\phi_1,\pi)] \tag{A5}$$

According to previous work, the coefficients a_n is determined by:

$$\sum_{n=0}^{\infty}(n+\frac{1}{2})b_{2n+1}\sin(n+\frac{1}{2})\theta=0,\quad \theta\in(0,\theta_0) \tag{A6}$$

$$\sum_{n=0}^{\infty}b_{2n+1}\sin(n+\frac{1}{2})\theta=E_0,\quad \theta\in(\theta_0,\pi) \tag{A7}$$

The equation of coefficient a_n is transfer to symmetrical triple series equations:

$$\sum_{n=0}^{\infty}(n+\frac{1}{2})b_{2n+1}\sin(n+\frac{1}{2})\theta=0,\quad \theta\in(0,\theta_0) \tag{A8a}$$

$$\sum_{n=0}^{\infty}b_{2n+1}\sin(n+\frac{1}{2})\theta=A_0,\quad \theta\in(\theta_0,\pi) \tag{A8b}$$

Previous works shows relation between a_n and b_n.[50] Hear $A_0=\left(\tan\phi_0\tan\phi_1\right)^{\frac{1}{2}}$, $\theta=4\arctan[\tan\phi(\tan\frac{1}{2}\phi_0\tan\frac{1}{2}\phi_1)^{-\frac{1}{2}}]$, and $\theta_0=4\arctan[(\tan\frac{1}{2}\phi_0\cot\frac{1}{2}\phi_1)^{\frac{1}{2}}]$. According to previous study, the b_{2n+1} is given by:[18]

$$b_{2n+1}=\left(\tan\frac{\phi_0}{2}\tan\frac{\phi_1}{2}\right)^{\frac{1}{2}}\left\{\left(n+\frac{1}{2}\right)K\left(\sqrt{\frac{1-\cos\theta_0}{2}}\right)\right\}^{-1}P_n(\cos\theta_0) \tag{A9}$$

Where $K(z)$ and P_n is the first kind complete elliptic integral and Jacobi polynomial. Thus, the potential can be determined. According to Poisson equation, the electric field of region ($\rho\le1$) is given by:[49]

$$E=-\nabla\varphi(\rho,\phi)=-(\frac{\partial\varphi}{\partial\rho}\hat{e}_\rho+\frac{1}{\rho}\frac{\partial\varphi}{\partial\phi}\hat{e}_\phi)=-\sum_{n=1}^{\infty}na_n\rho^{n-1}[\sin(n\phi)\hat{e}_\rho+\cos(n\phi)\hat{e}_\phi] \tag{A10}$$

Where $\hat{e}_\rho$ and $\hat{e}_\phi$ is the unit vector of electric field in polar coordinates. The electric field distribution is depended on the angle ϕ_0 and ϕ_1.

Received: ((will be filled in by the editorial staff))

Revised: ((will be filled in by the editorial staff))
Published online: ((will be filled in by the editorial staff))

References

[1] E. H. Kim, Y. Jo, S. Sai, M. J. Park, J. Y. Kim, J. S. Kim, Y. J. Lee, J. M. Cho, S. Y. Kwak, J. H. Baek, Y. K. Jeong, J. Y. Song, M. Yoon, S. G. Hwang, *Oncogene* **2019**, 38, 6630.

[2] a)E. D. Kirson, Z. Gurvich, R. Schneiderman, E. Dekel, A. Itzhaki, Y. Wasserman, R. Schatzberger, Y. Palti, *Cancer Res* **2004**, 64, 3288; b)E. D. Kirson, V. Dbaly, F. Tovarys, J. Vymazal, J. F. Soustiel, A. Itzhaki, D. Mordechovich, S. Steinberg-Shapira, Z. Gurvich, R. Schneiderman, Y. Wasserman, M. Salzberg, B. Ryffel, D. Goldsher, E. Dekel, Y. Palti, *Proc Natl Acad Sci U S A* **2007**, 104, 10152; c)E. D. Kirson, R. S. Schneiderman, V. Dbaly, F. Tovarys, J. Vymazal, A. Itzhaki, D. Mordechovich, Z. Gurvich, E. Shmueli, D. Goldsher, Y. Wasserman, Y. Palti, *BMC Med Phys* **2009**, 9, 1.

[3] a)A. A. Kanner, E. T. Wong, J. L. Villano, Z. Ram, E. F. Investigators, *Semin Oncol* **2014**, 41 Suppl 6, S25; b)G. Miesenbock, *Sci Am* **2008**, 299, 52.

[4] a)F. Fan, Z. Tian, Z. L. L. Wang, *Nano Energy* **2012**, 1, 328; b)Z. L. Wang, *Faraday Discuss* **2014**, 176, 447; c)Z. L. Wang, *Rep Prog Phys* **2021**, 84.

[5] a)Z. L. Wang, *ACS Nano* **2013**, 7, 9533; b)H. Wang, J. Cheng, Z. Wang, L. Ji, Z. L. Wang, *Sci Bull (Beijing)* **2020**, 66, 490; c)J. Luo, Z. Wang, *EcoMat* **2020**, 2, e12059; d)R. Hinchet, H. J. Yoon, H. Ryu, M. K. Kim, E. K. Choi, D. S. Kim, S. W. Kim, *Science* **2019**, 365, 491.

[6] Q. Zheng, B. Shi, Z. Li, Z. L. Wang, *Adv Sci (Weinh)* **2017**, 4, 1700029.

[7] a)F. Arab Hassani, R. P. Mogan, G. G. L. Gammad, H. Wang, S. C. Yen, N. V. Thakor, C. Lee, *ACS Nano* **2018**, 12, 3487; b)S. Lee, H. Wang, W. Peh, T. He, S. C. Yen, N. V. Thakor, C. Lee, *Nano Energy* **2019**, 60, 449.

[8] a)Y. Jin, J. Seo, J. S. Lee, S. Shin, H. J. Park, S. Min, E. Cheong, T. Lee, S. W. Cho, *Adv Mater* **2016**, 28, 7365; b)W. Hu, X. Wei, L. Zhu, D. Yin, A. Wei, X. Bi, T. Liu, G. Zhou, Y. Qiang, X. Sun, Z. Wen, Y. Pan, *Nano Energy* **2019**, 57, 600; c)G. Li, Q. Zhu, B. Wang, R. Luo, X. Xiao, Y. Zhang, L. Ma, X. Feng, J. Huang, X. Sun, Z. Wen, Y. Pan, C. Yang, *Adv Sci (Weinh)* **2021**, 8, e2100964.

[9] a)J. Wang, H. Wang, T. He, B. He, N. V. Thakor, C. Lee, *Adv. Sci.* **2019**, 6, 1900149; b)J. Wang, H. Wang, N. V. Thakor, C. Lee, *ACS Nano* **2019**, 13, 3589.

[10] a)J. Jang, J. Lee, J. H. Jang, H. Choi, *Adv Healthc Mater* **2016**, 5, 2481; b)H. Guo, X. Pu, J. Chen, Y. Meng, M. H. Yeh, G. Liu, Q. Tang, B. Chen, D. Liu, S. Qi, C. Wu, C. Hu, J. Wang, Z. L. Wang, *Sci Robot* **2018**, 3, eaat2516; c)Y. Liu, Y. Zhu, J. Liu, Y. Zhang, J. Liu, J. Zhai, *Nanoscale Res Lett* **2018**, 13, 191.

[11] a)Y. Dai, Y. Fu, H. Zeng, L. Xing, Y. Zhang, Y. Zhan, X. Xue, *Adv. Funct. Mater.* **2018**, 28, 1800275; b)M. Han, X. S. Zhang, X. Sun, B. Meng, W. Liu, H. Zhang, *Sci Rep* **2014**, 4, 4811.

[12] T. Zhong, M. Zhang, Y. Fu, Y. Han, H. Guan, H. He, T. Zhao, L. Xing, X. Xue, Y. Zhang, Y. Zhan, *Nano Energy* **2019**, 63, 103884.

[13] C. Zhao, H. Feng, L. Zhang, Z. Li, Y. Zou, P. Tan, H. Ouyang, D. Jiang, M. Yu, C. Wang, H. Li, L. L. Xu, W. Wei, Z. Li, *Adv. Funct. Mater.* **2019**, 29, 1808640.

[14] S. Yao, X. Zhao, X. Wang, T. Huang, Y. Ding, J. Zhang, Z. Zhang, Z. L. Wang, L. Li, *Adv Mater* **2022**, 34, e2109568.

[15] K. Fan, J. Hao, C. Wang, C. Zhang, W. Wang, F. Wang, *Energy Conversion and Management* **2021**, 241, 114301.

[16] Z. L. Wang, *Materials Today* **2017**, 20, 74.

[17] a)Z. L. Wang, *Materials Today* **2022**, 52, 348; b)Z. L. Wang, *Journal of Physics Communications* **2022**, 6, 085013; c)Z. L. Wang, *International Journal of Modern Physics B* **2022**, 37, 2350159.

[18] T. Chen, R. Bowle, N. Bowler, *Appl. Phys. Lett.* **2014**, 104, 032901.

[19] a)K. Dong, X. Peng, Z. L. Wang, *Adv Mater* **2020**, 32, e1902549; b)J. Wang, S. Li, F. Yi, Y. Zi, J. Lin, X. Wang, Y. Xu, Z. L. Wang, *Nat Commun* **2016**, 7, 12744.
[20] a)L. Zhang, H. Wang, X. Qu, *Advanced Materials* **2023**, n/a, 2211147; b)Z. Liu, X. Liang, H. Liu, Z. Wang, T. Jiang, Y. Cheng, M. Wu, D. Xiang, Z. Li, Z. L. Wang, L. Li, *ACS Nano* **2020**, 14, 15458; c)Z. Liu, J. Nie, B. Miao, J. Li, Y. Cui, S. Wang, X. Zhang, G. Zhao, Y. Deng, Y. Wu, Z. Li, L. Li, Z. L. Wang, *Advanced Materials* **2019**, 31, 1807795.
[21] a)J. Han, Y. Feng, P. Chen, X. Liang, H. Pang, T. Jiang, Z. L. Wang, *Advanced Functional Materials* **2022**, 32, 2108580; b)P. Chen, J. An, S. Shu, R. Cheng, J. Nie, T. Jiang, Z. L. Wang, *Advanced Energy Materials* **2021**, 11, 2003066; c)Z. Lin, B. Zhang, H. Zou, Z. Wu, H. Guo, Y. Zhang, J. Yang, Z. L. Wang, *Nano Energy* **2020**, 68, 104378; d)J. Wang, W. Ding, L. Pan, C. Wu, H. Yu, L. Yang, R. Liao, Z. L. Wang, *ACS Nano* **2018**, 12, 3954.
[22] R. Mahdavi, P. Hosseinpour, F. Abbasvandi, S. Mehrvarz, N. Yousefpour, H. Ataee, M. Parniani, A. Mamdouh, H. Ghafari, M. Abdolahad, *Biosensors and Bioelectronics* **2020**, 165, 112421.
[23] Q. M. Saqib, R. A. Shaukat, M. Y. Chougale, M. U. Khan, J. Kim, J. Bae, *Nano Energy* **2022**, 100, 107475.
[24] J. H. Park, C. Wu, S. Sung, T. W. Kim, *Nano Energy* **2019**, 57, 872.
[25] a)G. Qi, B. Wang, X. Song, H. Li, Y. Jin, *National Science Review* **2020**, 7, 660; b)G. Qi, B. Wang, Y. Zhang, H. Li, C. Li, W. Xu, Y. Jin, *Analytical Chemistry* **2019**, 91, 9571; c)G. Qi, H. Li, Y. Zhang, C. Li, S. Xu, M. Wang, Y. Jin, *Analytical Chemistry* **2019**, 91, 1408.
[26] a)G. Qi, D. Wang, C. Li, K. Ma, Y. Zhang, Y. Jin, *Analytical Chemistry* **2020**, 92, 11755; b)G. Qi, M. Zhang, J. Tang, Y. Jin, *Advanced Science* **2023**, 10, 2207165.
[27] B. Chu, X. Qin, Q. Zhu, H. Wang, Z. Wen, X. Sun, Y. He, S.-T. Lee, *Nano Energy* **2022**, 100, 107471.
[28] a)H. Ryu, J. H. Lee, U. Khan, S. S. Kwak, R. Hinchet, S.-W. Kim, *Energy & Environmental Science* **2018**, 11, 2057; b)D. Liu, X. Yin, H. Guo, L. Zhou, X. Li, C. Zhang, J. Wang, Z. L. Wang, *Science Advances*, 5, eaav6437; c)Z. Zhao, L. Zhou, S. Li, D. Liu, Y. Li, Y. Gao, Y. Liu, Y. Dai, J. Wang, Z. L. Wang, *Nature Communications* **2021**, 12, 4686.
[29] a)M. Zheng, S. Lin, Z. Tang, Y. Feng, Z. L. Wang, *Nano Energy* **2021**, 83, 105810; b)M. Zheng, S. Lin, L. Xu, L. Zhu, Z. L. Wang, *Advanced Materials* **2020**, 32, 2000928; c)L. Ren, A. Yu, W. Wang, D. Guo, M. Jia, P. Guo, Y. Zhang, Z. L. Wang, J. Zhai, *Nano Letters* **2021**, 21, 10099.
[30] J. Wang, Y. Li, Z. Xie, Y. Xu, J. Zhou, T. Cheng, H. Zhao, Z. L. Wang, *Advanced Energy Materials* **2020**, 10, 1904227.
[31] a)R. Yang, M. Benner, Z. Guo, C. Zhou, J. Liu, *Advanced Functional Materials* **2021**, 31, 2103132; b)C. Ma, B. Kim, S.-W. Kim, N.-G. Park, *Energy & Environmental Science* **2021**, 14, 374; c)Y.-S. Lee, S. Jeon, D. Kim, D.-M. Lee, D. Kim, S.-W. Kim, *Nano Energy* **2023**, 106, 108066.
[32] H. Wu, L. Yang, H. Liu, D. Zhou, D. Chen, X. Zheng, H. Yang, C. Li, J. Chang, A. Wu, Z. Wang, N. Ren, S. Lv, Y. Liu, M. Jia, J. Lu, H. Liu, G. Sun, Z. Liu, J. Liu, L. Chen, *CNS Neuroscience & Therapeutics* **2021**, 27, 1587.
[33] a)E. D. Kirson, V. Dbalý, F. Tovaryš, J. Vymazal, J. F. Soustiel, A. Itzhaki, D. Mordechovich, S. Steinberg-Shapira, Z. Gurvich, R. Schneiderman, Y. Wasserman, M. Salzberg, B. Ryffel, D. Goldsher, E. Dekel, Y. Palti, *Proceedings of the National Academy of Sciences* **2007**, 104, 10152; b)A. F. Kessler, G. E. Frömbling, F. Gross, M. Hahn, W. Dzokou, R.-I. Ernestus, M. Löhr, C. Hagemann, *Cell Death Discovery* **2018**, 4, 77.
[34] S. W. Tait, D. R. Green, *Nat Rev Mol Cell Biol* **2010**, 11, 621.

[35] C. N. M. Ryan, M. N. Doulgkeroglou, D. I. Zeugolis, *BMC Biomed Eng* **2021**, 3, 1.
[36] a)X. Zhang, L. Li, J. Ouyang, L. Zhang, J. Xue, H. Zhang, W. Tao, *Nano Today* **2021**, 39, 101196; b)G. Yao, D. Jiang, J. Li, L. Kang, S. Chen, Y. Long, Y. Wang, P. Huang, Y. Lin, W. Cai, X. Wang, *ACS Nano* **2019**, 13, 12345.
[37] S. Zhong, S. Yao, Q. Zhao, Z. Wang, Z. Liu, L. Li, Z. L. Wang, *Advanced NanoBiomed Research* **2023**, 3, 2200143.
[38] D. Fabian, M. D. Guillermo Prieto Eibl, I. Alnahhas, N. Sebastian, P. Giglio, V. Puduvalli, J. Gonzalez, J. D. Palmer, *Cancers*, 10.3390/cancers11020174
[39] M. Zhou, M. Huang, H. Zhong, C. Xing, Y. An, R. Zhu, Z. Jia, H. Qu, S. Zhu, S. Liu, L. Wang, H. Ma, Z. Qu, G. Ning, S. Feng, *Advanced Functional Materials* **2022**, 32, 2200269.
[40] I. Shlomy, S. Divald, K. Tadmor, Y. Leichtmann-Bardoogo, A. Arami, B. M. Maoz, *ACS Nano* **2021**, 15, 11087.
[41] B. Wang, G. Li, Q. Zhu, W. Liu, W. Ke, W. Hua, Y. Zhou, X. Zeng, X. Sun, Z. Wen, C. Yang, Y. Pan, *Small* **2022**, 18, 2201056.
[42] S. Yao, S. Wang, M. Zheng, Z. Wang, Z. Liu, Z. L. Wang, L. Li, *Advanced Materials* **2023**, 35, 2303962.
[43] S. Zhong, C. Xiong, Y. Zhao, S. Yao, Q. Hu, S. Wang, Q. Zhao, L. Li, *Advanced Functional Materials* **2023**, 2305625.
[44] a)P. Zhu, B. Zhang, H. Wang, Y. Wu, H. Cao, L. He, C. Li, X. Luo, X. Li, Y. Mao, *Nano Research* **2022**, 15, 7460; b)Y. Liu, Y. Zheng, Z. Wu, L. Zhang, W. Sun, T. Li, D. Wang, F. Zhou, *Nano Energy* **2021**, 79, 105422; c)Z. Liu, Y. Ma, H. Ouyang, B. Shi, N. Li, D. Jiang, F. Xie, D. Qu, Y. Zou, Y. Huang, H. Li, C. Zhao, P. Tan, M. Yu, Y. Fan, H. Zhang, Z. L. Wang, Z. Li, *Advanced Functional Materials* **2019**, 29, 1807560.
[45] a)Q. Chen, W. Deng, J. He, L. Cheng, P.-G. Ren, Y. Xu, **2022**, 10; b)G. Liu, S. Xu, Y. Liu, Y. Gao, T. Tong, Y. Qi, C. Zhang, *Advanced Functional Materials* **2020**, 30, 1909886.
[46] D. Zhao, J. Zhuo, Z. Chen, J. Wu, R. Ma, X. Zhang, Y. Zhang, X. Wang, X. Wei, L. Liu, C. Pan, J. Wang, J. Yang, F. Yi, G. Yang, *Nano Energy* **2021**, 90, 106580.
[47] L. Guan, P. Fan, X. Liu, R. Liu, Y. Liu, H. Bai, *Front Cell Dev Biol* **2021**, 9, 724012.
[48] X. Meng, X. Xiao, S. Jeon, D. Kim, B.-J. Park, Y.-J. Kim, N. Rubab, S. Kim, S.-W. Kim, *Advanced Materials* **2023**, 35, 2209054.
[49] H. Kamberaj, *Electromagnetism: With Solved Problems*, Springer Cham, **2022**.
[50] S. Vinogradov, P. Smith, E. Vinogradova, *Canonical problems in scattering and potential theory part II: Acoustic and electromagnetic diffraction by canonical structures*, CRC Press, **2002**.